JOURNAL OF MATERIALS SCIENCE 30 (1995) 1500–1510

Correlations between gas phase supersaturation, nucleation process and physico-chemical characteristics of silicon carbide deposited from Si–C–H–Cl system on silica substrates

D. LESPIAUX, F. LANGLAIS, R. NASLAIN
Laboratoire des Composites Thermostructuraux, UMR 47 CRNS-SEP-UB1 Domaine Universitaire, 3 Allée de la Boëtie, 33600 Pessac, France

S. SCHAMM, J. SEVELY
Centre d'Elaboration de Matériaux et d'Etudes Structurales, Laboratoire d'Optique Electronique, UPR 8011 CNRS, BP 4347, 31055 Toulouse Cedex, France

In the CH_3SiCl_3–H_2 CVD system, from which SiC-based films are prepared, the supersaturation of the gas phase increases when temperature and total pressure decreases and when a diffusion-controlled kinetic process is changed in a reaction-controlled one. These conditions variations seem to induce a transition from a growth regime to a nucleation regime, as evidenced by a study of the initial stages of the deposition. A transition from a crystallized film with columnar crystals to a nanocrystalline deposit is also reported on the basis of accurate experiments using TEM and related techniques.

1. Introduction

Silicon carbide-based ceramics are increasingly applied as semiconducting components of microelectronic devices and matrices of thermostructural fibrous composite materials. Their electrical and mechanical properties are highly dependent on their physico-chemical characteristics at a microscopic scale and their processing technique. Chemical vapour deposition (CVD) is a very suitable method for preparing semiconducting thin films and the derived chemical vapour infiltration (CVI) technique is well adapted to the processing of ceramic matrix composites [1, 2]. A variety of SiC-based ceramics (in terms of microstructure or local chemical composition) can be prepared by varying the experimental conditions within a relatively narrow range [3–5].

In the field of silicon deposition, the initial nucleation processes are known to play a decisive role in the grain size control of polycrystalline layers [6–11]. The various factors which can influence the nucleation characteristics have been studied, such as temperature, gas phase composition, adsorption of different species, nature of the substrate. Among these factors, the supersaturation of the gas phase close to the substrate is considered as a parameter which controls the nucleation process, but it has not been quantitatively studied. On the other hand, the nucleation approaches have not been frequently connected to a precise description of the thin films from a micro- or nanostructural point of view.

Several papers concerning silicon carbide CVD deal with the morphological characteristics of the thin layers [12–14], but the contributions of the gas phase supersaturation and the nucleation process have never been investigated. The aim of the present article is to state correlations between SiC synthesis conditions and physicochemical characteristics of SiC films through (i) estimations of supersaturation under various kinetic conditions, (ii) a study of the nucleation process and (iii) an accurate chemical and microstructural characterization of the films. The SiC precursor is CH_3SiCl_3(MTS)–H_2 gaseous mixture and the nucleation and growth experiments were performed on amorphous SiO_2 substrates whose surface is well defined and does not exhibit preferred nucleation sites at a microscopic scale (scanning electron microscopy, SEM).

2. Assessments of gas phase supersaturation

2.1. Definition, calculation procedure and kinetic considerations

According to Cadoret [15], any heterogeneous reaction leading to the growth of SiC may be chosen for the calculation of the supersaturation of the gas phase (which represents the departure from equilibrium and can control the nucleation process). A previous work has pointed out that CH_3SiCl_3 was decomposed in the

0022–2461

gas phase according to the following reaction

$$CH_3SiCl_3 + H_2 \rightarrow CH_4 + SiCl_2 + HCl \quad (1)$$

and the heterogeneous deposition reaction could be [16]

$$CH_4 + SiCl_2 \rightarrow SiC_{(s)} + 2HCl + H_2 \quad (2)$$

The Gibbs free energy variation for this reaction at a growth site of the solid surface is given by

$$\Delta G = \Delta G^\circ + RT \log\left(\frac{P_{H_2} P_{HCl}^2}{P_{CH_4} P_{SiCl_2}}\right) \quad (3)$$

where ΔG° is the standard Gibbs free energy variation and P_{H_2}, P_{HCl}, P_{CH_4} and P_{SiCl_2} the partial pressures close to the solid surface, R the perfect gas constant and T the temperature in K. Under heterogeneous equilibrium conditions

$$\Delta G^\circ = -RT \log\left(\frac{P_{H_2} P_{HCl}^2}{P_{CH_4} P_{SiCl_2}}\right)_{equ} = -RT \log K_p(T) \quad (4)$$

where $K_p(T)$ is the equilibrium constant corresponding to the Equation 2. Thus

$$\Delta G = -RT \log\left(\frac{P_{CH_4} P_{SiCl_2}}{P_{H_2} P_{HCl}^2} K_p(T)\right) \quad (5)$$

The supersaturation γ is defined by

$$\Delta G = -RT \log(1 + \gamma) \quad (6)$$

which means

$$\gamma = \frac{P_{CH_4} P_{SiCl_2}}{P_{H_2} P_{HCl}^2} K_p(T) - 1 \quad (7)$$

If $\gamma > 0$, $\Delta G < 0$ and the deposition reaction is more and more irreversible as the supersaturation is higher.

The equilibrium constant $K_p(T)$ can be directly calculated from the thermodynamic data (enthalpies and entropies of formation) of each species (Si, C and SiC solid phases and 22 gas species of the Si–C–H–Cl system) by minimizing the overall Gibbs free energy of the system. The calculations of the partial pressures near the substrate require assumptions on the kinetic process.

The first case, which frequently occurs, corresponds to deposition kinetics controlled by the surface reactions. In this case, which is usually favoured by decreasing the temperature and the total pressure and increasing the total flow rate, the local composition of the gas phase can be assumed to be given by the homogeneous gas phase equilibrium, being supposed to be reached very rapidly with respect to the heterogeneous one. This hypothesis is particularly valid here, since the deposition proceeds in a hot-wall reactor with a large isothermal reactional area. Under these conditions, the boundary layer does not occur, the supersaturation can be well defined close to the substrate and calculated according to Equation 7. The calculation procedure for the homogeneous partial pressures is the same as for the heterogeneous ones. The only difference comes from the fact that the condensed phases are not introduced in the system.

In the second case, when the deposition kinetics is governed by the mass transport, i.e. the diffusion of the gaseous species through a boundary layer occurring all around the substrate, the supersaturation cannot be calculated within the stagnant gas layer, but only outside. Due to the occurrence of concentration gradients, the local supersaturation very close to the solid surface is almost zero (i.e. the heterogeneous equilibrium may give a valid estimate of the gas phase composition at the surface).

As a consequence, before interpreting the nucleation results on the basis of supersaturation calculations, it is important to know the type of kinetic regime. Very recently an experimental study of the SiC deposition rates, carried out in the same CVD reactor, has permitted us to derive the conditions (i.e. pressure and temperature) favourable to a mass transfer or a surface reaction governed kinetic process [17].

Finally, the supersaturation was calculated under the assumption of rapid homogeneous reactions, outside the boundary layer if it exists and for conditions of pure SiC deposition, as determined previously [15] in terms of temperature, total pressure and dilution ratio α

$$1073 \leq T \leq 1473 \text{ K}, \qquad 3 \leq P \leq 50 \text{ kPa}$$

and

$$10 \leq \alpha \leq 100.$$

2.2. Results and discussion

The supersaturation of the gas phase, calculated as defined above, is plotted as a function of the temperature and pressure in Figs 1 and 2.

Except for a highly diluted gas phase ($\alpha = 100$) for which temperature does not have a great influence, the supersaturation decreases with increasing temperature (Fig. 1), which is consistent with the increase of P_{HCl} and the decrease of P_{CH_4} already calculated in the hypothesis of the homogeneous equilibrium [15]. Similar variations were computed in a previous work dealing with silicon growth from SiH_2Cl_2–H_2 system [18].

The total pressure has almost the same influence as the temperature (Fig. 2). The continuous decrease of γ when P increases can be explained on the basis of the increase of H_2 and HCl homogeneous partial pressures [15].

As shown in Fig. 1, the variations of the supersaturation with the dilution ratio α depend on the temperature. At low temperatures ($T < 1150\,^\circ$C), a dilution of the gas phase results in a decrease of the supersaturation, while at higher temperatures, a slight increase is observed. At low temperatures, the calculation of the homogeneous equilibrium yields CH_4 and $SiCl_2$ partial pressures higher than HCl for low α values and lower for high α values [19], which can explain the decrease of the supersaturation when α rises, according to Equation 7. At high temperatures,

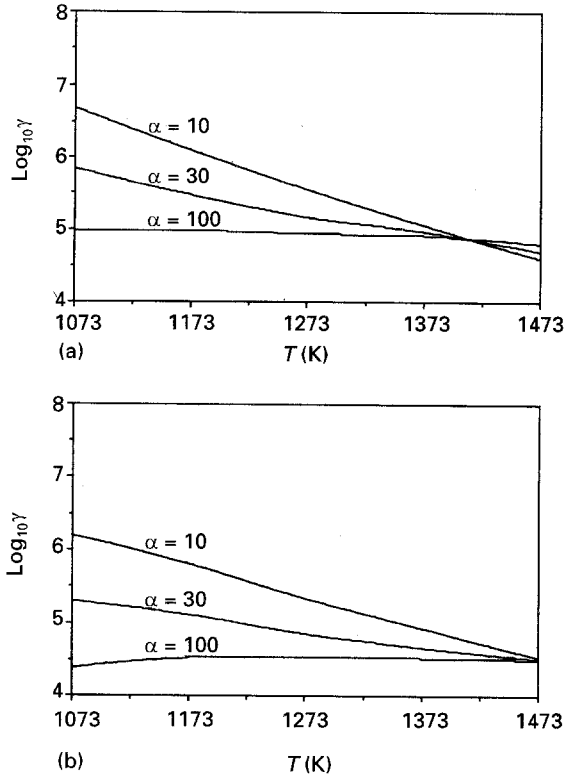

Figure 1 Variations of the calculated supersaturation γ versus temperature T at various α ratios for (a) $P = 20$ kPa and (b) $P = 50$ kPa.

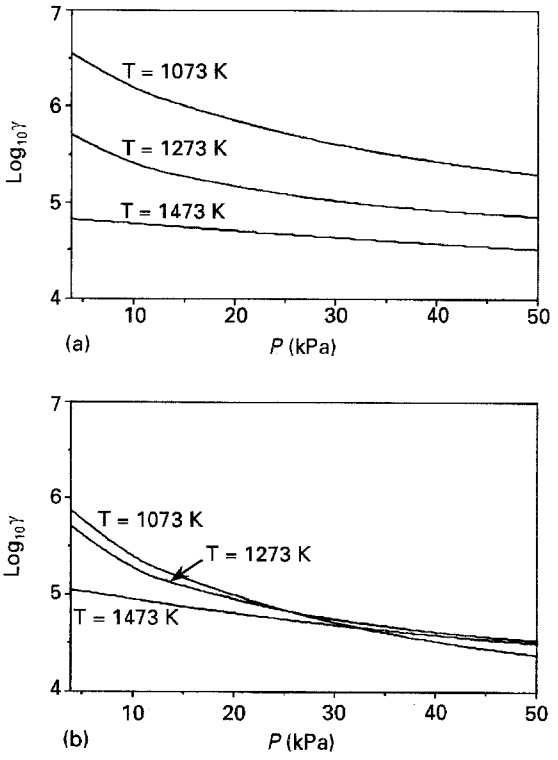

Figure 2 Variations of the calculated supersaturation γ versus total pressure P at various temperatures for (a) $\alpha = 30$ and (b) $\alpha = 100$.

the influence of α on the homogeneous partial pressures of the predominant species is not so important, which results in a weak influence on the supersaturation.

In conclusion, the SiC deposition process from MTS–H_2 system is highly irreversible, with supersaturation values higher than 10^4. It is still more irreversible than for the SiH_2Cl_2–H_2 system used for silicon growth.

3. Experimental procedure

3.1. Nucleation and growth experiments

The deposition experiments were performed in a vertical hot-wall CVD reactor working under reduced pressure and heated by r.f. induction (Fig. 3). The deposition chamber is a cylindrical glass silica tube favourable to a laminar flow, with a large hot isothermal zone. The reactor is equipped with systems for the accurate monitoring of temperature, total pressure and flow rates. MTS, which is liquid under standard conditions, is transported to the reactor by bubbling the carrier gas H_2 in a vessel at a constant temperature. A good control of the MTS gas flow needs additional devices, which have been described elsewhere [16]. The initial composition of the gas phase is given by the ratio α between H_2 and MTS partial pressures P_i or flow rates Q_i (with i = H_2 or MTS)

$$\alpha = \frac{P_{H_2}}{P_{MTS}} = \frac{Q_{H_2}}{Q_{MTS}} \quad (8)$$

A microbalance is used to acquire the deposition rates (Fig. 3). It is protected from corrosive gas upstream by a counter-flow of hydrogen which is added to the main stream of carrier gas. An interface with a microcomputer is used to follow continuously the kinetics of the process and to store all the mass and time data. Thus, the curves giving mass versus time, can be drawn and transient and steady-state stages can be evidenced.

The amorphous SiO_2 substrates used for the nucleation and growth experiments, were obtained by oxidizing silicon wafers in air at 900 °C for 30 h. The silica layer is about 500 nm in thickness and exhibits a very uniform external surface.

Very short experiments (usually less than one minute) were carried out to follow the nucleation process. The study of the initial stages of SiC deposition is mainly based on measurement of the density of nuclei as a function of time. These nuclei can be observed on SEM micrographs as shown in Fig. 4. In most cases, a high density of nuclei is obtained after a very short time, which means a very high nucleation rate, I (Fig. 4a). Then, this density reaches a maximum value (referred to as the saturation density, N_S) and the size of nuclei is increased up to the saturation nucleus size, Φ_S (Fig. 4b). At last, coalescence occurs with a decrease in nucleus density (Fig. 4c). Fig. 5 shows typical examples of nucleation curves, where the nucleus density is plotted as a function of time for various CVD conditions. Three characteristics can be derived from these nucleation experiments: the nucleation rate I, the saturation nucleus density N_S and the saturation nucleus size Φ_S.

3.2. Physico-chemical characterization of the films

A first microstructural approach of the SiC-based thin films was carried out by SEM and X-ray diffraction (XRD).

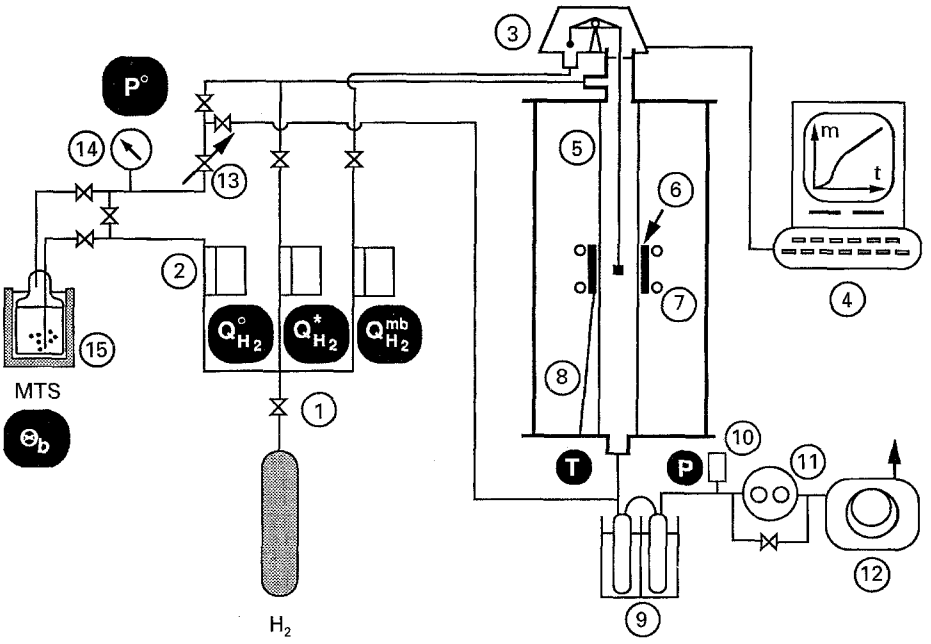

Figure 3 Schematics of the apparatus used for CVD/CVI of SiC-based ceramics. 1, shut-off valve; 2, mass flowmeter; 3, microbalance; 4, microcomputer; 5, silica tubular reactor; 6, susceptor; 7, r.f. coil; 8, thermocouple; 9, liquid nitrogen trap; 10, pressure sensor; 11, pressure controller; 12, vacuum pump; 13, adjusting value; 14, manometer ($P°$); 15, thermostatted bath ($P°$ MTS).

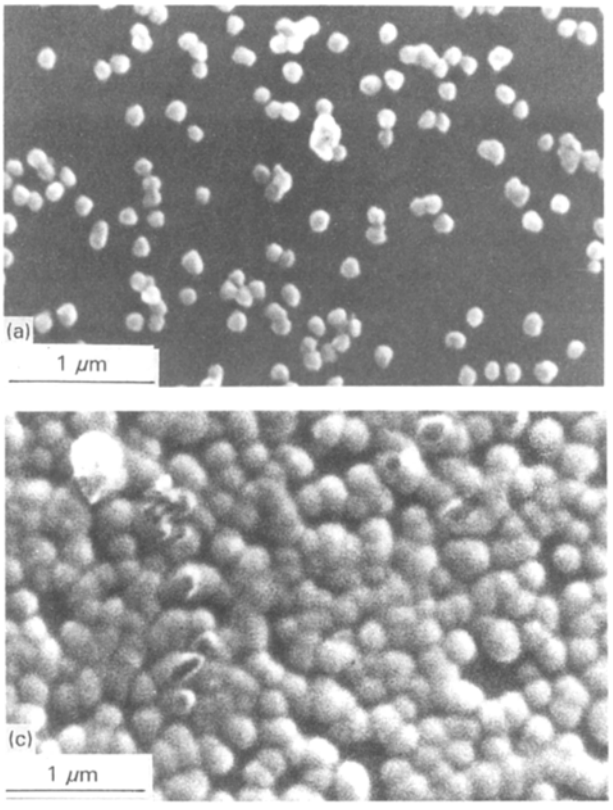

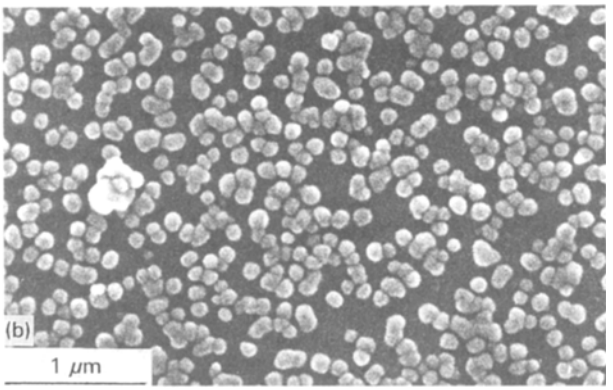

Figure 4 SEM pictures of the nucleus density at $T = 1100\,°C$, $\alpha = 30$ and $P = 3\,kPa$ deposited on a SiO_2 substrate after an exposure time of (a) 8 s, (b) 45 s and (c) 90 s.

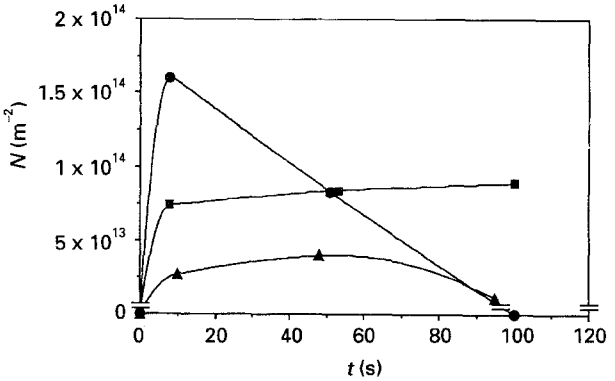

Figure 5 Variations of the nucleus density N versus deposition duration t for three different CVD conditions. ■, $T = 900\,°C$, $\alpha = 30$, $P = 20\,kPa$, $Q = 200$ sccm; ●, $T = 900\,°C$, $\alpha = 3$, $P = 3\,kPa$, $Q = 200$ sccm. ▲, $T = 1100\,°C$, $\alpha = 30$, $P = 3\,kPa$, $Q = 200$ sccm.

Transmission electron microscopy (TEM) (bright-field and dark-field observations and selected area electron diffraction) combined to electron energy loss spectroscopy (EELS) were used for a description of the SiC-based films at a nanometric scale. The samples were prepared by mechanical polishing and ion thinning.

All specimens were examined in a transmission electron microscope (CM30-ST from Philips) equipped with a PEELS spectrometer (Gatan) for parallel electron energy loss spectroscopy. Probe size was 60 nm and only 30 nm for analysing the nuclei or the very thin layers.

The local chemical organization of the films was investigated by using core excitation signals. The low energy Si–L core loss edge (99 eV), the C–K edge (284 eV) and the O–K edge (532 eV) have been considered for EELS analysis. The quantitative analysis of the samples has been possible with stoichiometric silicon carbide as a reference material.

4. Nucleation process

The gas phase supersaturation was calculated and the nucleation characteristics were measured for various experimental conditions. The nucleation rate I is drawn in Fig. 6 on a log-log scale as a function of the supersaturation γ calculated outside the boundary layer if it exists. I is proportional to $\gamma^{0.7}$ for $\gamma > 10^5$. A transition seems to occur for $\gamma \approx 10^5$, which corresponds to the conditions $\alpha = 3$, $T = 1100\,^{\circ}C$ and $P = 20$ kPa. Similar variations of the saturation nucleus density N_S versus supersaturation are observed (Fig. 7), with a transition at the same γ value. The saturation nucleus size Φ_S decreases when γ increases, except for $\gamma \leq 10^5$ where the nucleus shape is different, which makes difficult the determination of Φ_S (Fig. 8).

For the high supersaturation values ($\gamma \approx 10^6$), the SiC nucleation characteristics exhibit a behaviour in good accordance with those observed for metals or semiconductors such as silicon [8, 20]. Conversely, a transition towards a very different nucleation process is pointed out for $\gamma < 10^5$. This behaviour can be explained by considering the kinetic effects on the local supersaturation. On the basis of kinetic data recently determined [16, 17], most of the nucleation experiments can be considered to have been performed under a reaction-controlled kinetic regime. The conditions defined by $T = 1100\,^{\circ}C$ and $P = 20$ kPa, which correspond to the lowest calculated supersaturations ($\gamma \leq 10^5$), favours a kinetic process governed by the mass transport by diffusion through a boundary layer. As a consequence, under these specific conditions, the calculated supersaturation is correct outside the boundary layer, but close to the deposition surface it is very much lower, which can explain the marked change in the nucleation process. The transition observed in terms of nucleation rate, saturation nucleus density and saturation nucleus size, must be correlated to the transition between both types of kinetic regimes, which results in a large drop of local supersaturation.

This transition is also evidenced by observing the growing nuclei by SEM. Under most conditions, the shape of the nuclei is almost hemispherical, without facet, as shown in Fig. 4. Only the mean diameters vary with the conditions of supersaturation. But when moving towards a diffusion-governed kinetic process, the morphological characteristics of the nuclei are drastically changed: acicular shapes grow, which probably means higher crystallite sizes (Fig. 9). This result is consistent with the shift to a very low local supersaturation of the gas phase due to the boundary layer, which favours a growth regime with respect to a nucleation regime.

In order to confirm and detail the microstructure of the nuclei formed in the nucleation regime, i.e. for high supersaturation, bright-field TEM observations were performed for $T = 1100\,^{\circ}C$, $\alpha = 30$, $P = 3$ kPa (close to conditions of point (b) in Figs 6, 7 and 8) and a process duration of 90 s (Fig. 10). The formation and coalescence of nanocrystallized hemispherical nuclei, about 150 nm in diameter, show that the high

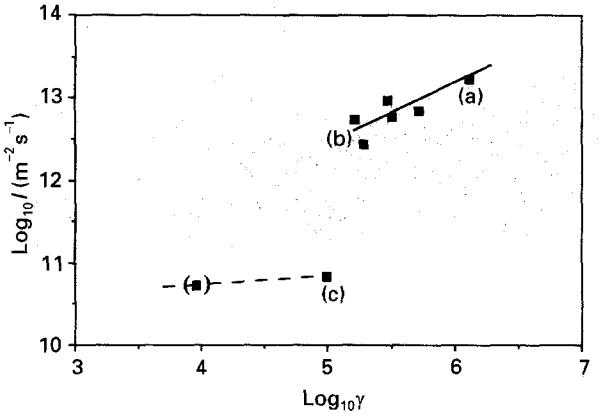

Figure 6 Variations of the nucleation rate I versus calculated supersaturation γ. (a) $T = 900\,^{\circ}C$, $\alpha = 3$, $P = 3$ kPa, (b) $T = 1100\,^{\circ}C$, $\alpha = 10$, $P = 3$ kPa and (c) $T = 1100\,^{\circ}C$, $\alpha = 3$, $P = 20$ kPa.

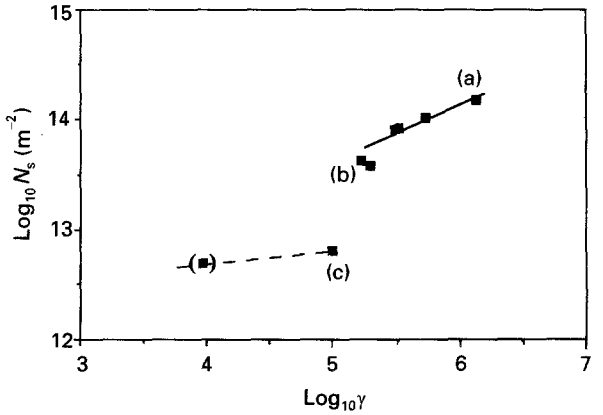

Figure 7 Variations of the saturation nucleus density N_s versus calculated supersaturation γ: (a) $T = 900\,^{\circ}C$, $\alpha = 3$ kPa, (b) $T = 1100\,^{\circ}C$, $\alpha = 10$, $P = 3$ kPa and (c) $T = 1100\,^{\circ}C$, $\alpha = 3$, $P = 20$ kPa.

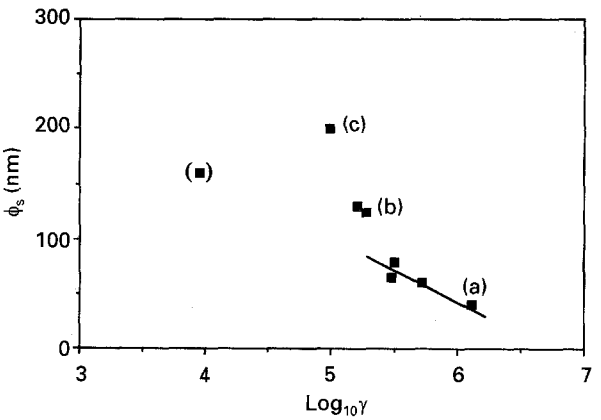

Figure 8 Variations of the mean size Φ_S of the nuclei, measured at saturation density versus calculated supersaturation γ: (a) $T = 900\,^{\circ}C$, $\alpha = 3$, $P = 3$ kPa, (b) $T = 1100\,^{\circ}C$, $\alpha = 10$, $P = 3$ kPa and (c) $T = 1100\,^{\circ}C$, $\alpha = 3$, $P = 20$ kPa.

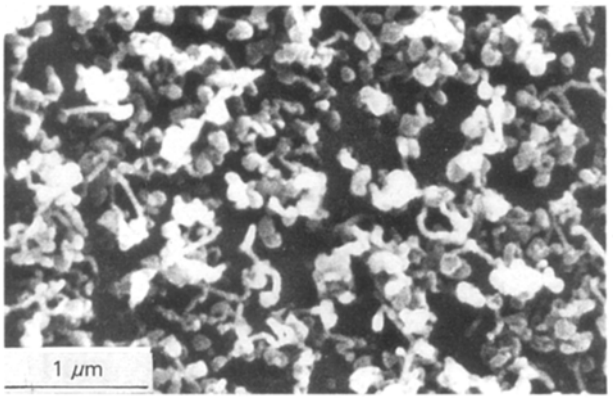

Figure 9 SEM picture of SiC-based nuclei deposited on a SiO_2 substrate after an exposure time of 90 s for $T = 1100\,°C$, $\alpha = 30$ and $P = 20\,kPa$.

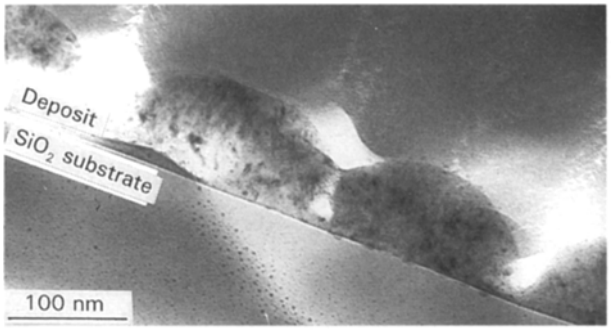

Figure 10 Bright-field image of SiC-based nuclei deposited on a SiO_2 substrate for $T = 1100\,°C$, $\alpha = 30$ and $P = 3\,kPa$.

supersaturation close to the surface inhibits the growth of crystals and is favourable to a smooth surface deposit.

5. Growth process and thin film analysis

Analyses of the SiC-based films were carried out for three typical experimental conditions. Conditions (a) ($T = 900\,°C$, $\alpha = 3$ and $P = 3\,kPa$) correspond to a high supersaturation, a reaction-controlled kinetics and a nucleation regime. Conditions (b) ($T = 1100\,°C$, $\alpha = 10$ and $P = 3\,kPa$) are associated with a kinetic process intermediate between a reaction and a transfer controlled regime with a lower supersaturation. Under conditions (c) ($T = 1100\,°C$, $\alpha = 3$ and $P = 20\,kPa$), the kinetic process is governed by the mass transport through a gaseous boundary layer and consequently the local supersaturation is very low.

5.1. Deposition kinetics

The curves showing the variations of the sample mass versus time are reported in Fig. 11 for conditions (a), (b) and (c). For the highest supersaturations conditions (a) and (b), a relatively long time (20–40 min) is needed to reach the steady state (5–2.5 $\mu m\,h^{-1}$). During the transient stage, the deposition rate increases continuously with time. Conversely, for conditions (c),

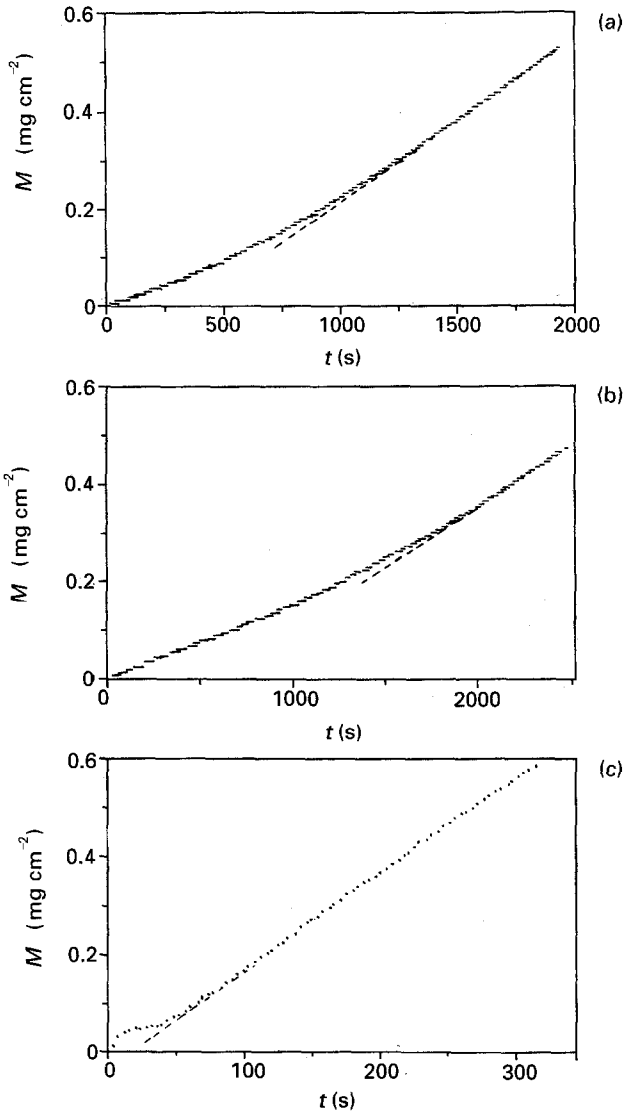

Figure 11 Mass–time curves recorded during SiC-based ceramics deposition on SiO_2 substrate for various conditions: (a) $T = 900\,°C$, $\alpha = 3$, $P = 3\,kPa$, (b) $T = 1100\,°C$, $\alpha = 10$, $P = 3\,kPa$ and (c) $T = 1100\,°C$, $\alpha = 3$, $P = 20\,kPa$.

i.e. for the lowest supersaturation, the steady state occurs very rapidly and the deposition rate is higher than for the other conditions ($25\,\mu m\,h^{-1}$) (Fig. 11c).

5.2. Surface morphology

The surface morphology of the films is highly dependent on the gas phase supersaturation (Fig. 12). The roughness increases as the supersaturation decreases. This type of correlation has been already mentioned, but only in terms of temperature, and to a lesser extent total pressure, whose decrease was known to favour a smooth surface [12–14, 21–24]. For conditions (c), with diffusion-controlled kinetics, an angular morphology is observed (Fig. 12c), which is consistent with a crystal growth regime due to the very low supersaturation. Similar morphology changes versus kinetic regime, were recently reported for the deposition of boron nitride from BF_3–NH_3 precursor [25].

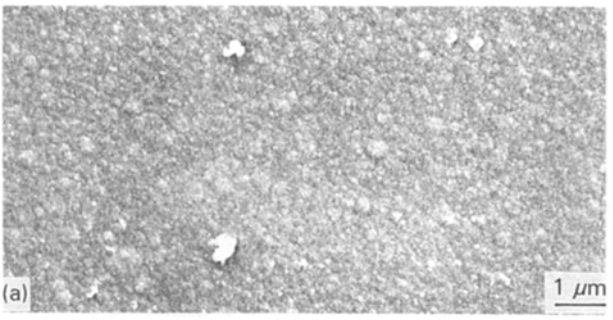

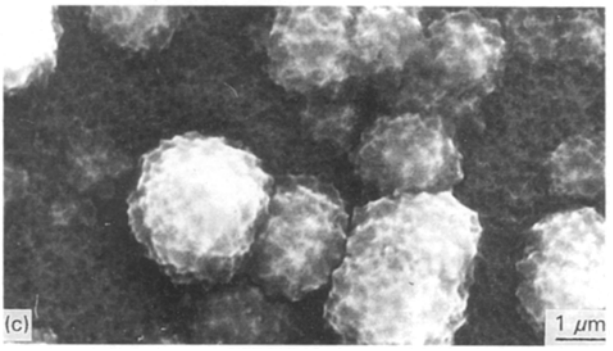

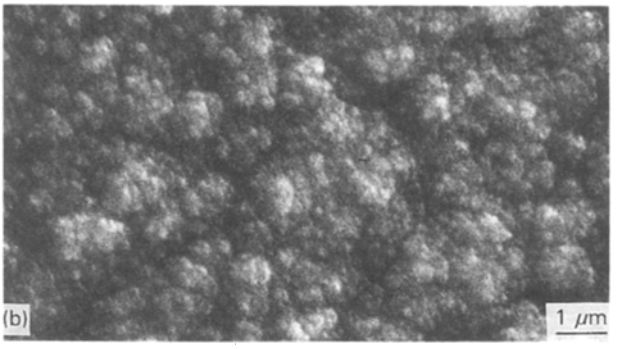

Figure 12 SEM pictures showing the morphological change of SiC-based deposits obtained under various conditions: (a) $T = 900\,°C$, $\alpha = 3$, $P = 3\,kPa$, (b) $T = 1100\,°C$, $\alpha = 10$, $P = 3\,kPa$, (c) $T = 1100\,°C$, $\alpha = 3$, $P = 20\,kPa$.

5.3. Structural properties

For the highest supersaturation value (conditions (a)), the TEM bright-field image (performed on films of $\approx 2\,\mu m$ in thickness) shows a quasi-amorphous material, which is confirmed by the corresponding electron diffraction and XRD patterns (Figs 13 and 14). A mean crystal size of about 1.5 nm can be deduced from the ring broadness [26]. The smooth surface morphology of the film is one of the consequences of this nanostructure (Fig. 12a).

Conditions (b), associated with a lower supersaturation, result in a film nanostructure which changes when moving from the interface with the substrate to the external surface. Fig. 15 shows dark-field images obtained by selecting with the objective aperture a part of the first ring. In the first observation, carried out close to the substrate, a nanocrystalline material is evidenced, with isotropic grains 5 nm in size (Fig. 15a). If observed at 1 μm far from the substrate, an anisotropy occurs giving rise to a slight columnar microstructure (Fig. 15b). As a consequence, some surface roughness can be observed (Fig. 12b).

Under conditions (c), i.e. for a very low supersaturation and a kinetic process limited by the mass transport, the microstructure of the film is rather complex, as shown in the bright-field image of Fig. 16a. On the SiO_2 substrate, after a nanocrystalline layer of only 30 nm in thickness, a more crystallized layer, whose thickness varies from 100 to 250 nm, is observed, with columnar crystallites highly developed perpendicular to the substrate, as confirmed by the narrowing of the (1 1 1) XRD line shown in Fig. 14. Then, quasi-circular and poorly crystallized inclusions occur, from which columnar crystallites similar to the above mentioned ones, grow in all directions (Fig. 16a and b), resulting in a star microstructure. In order to explain these structural heterogeneities, which can result in

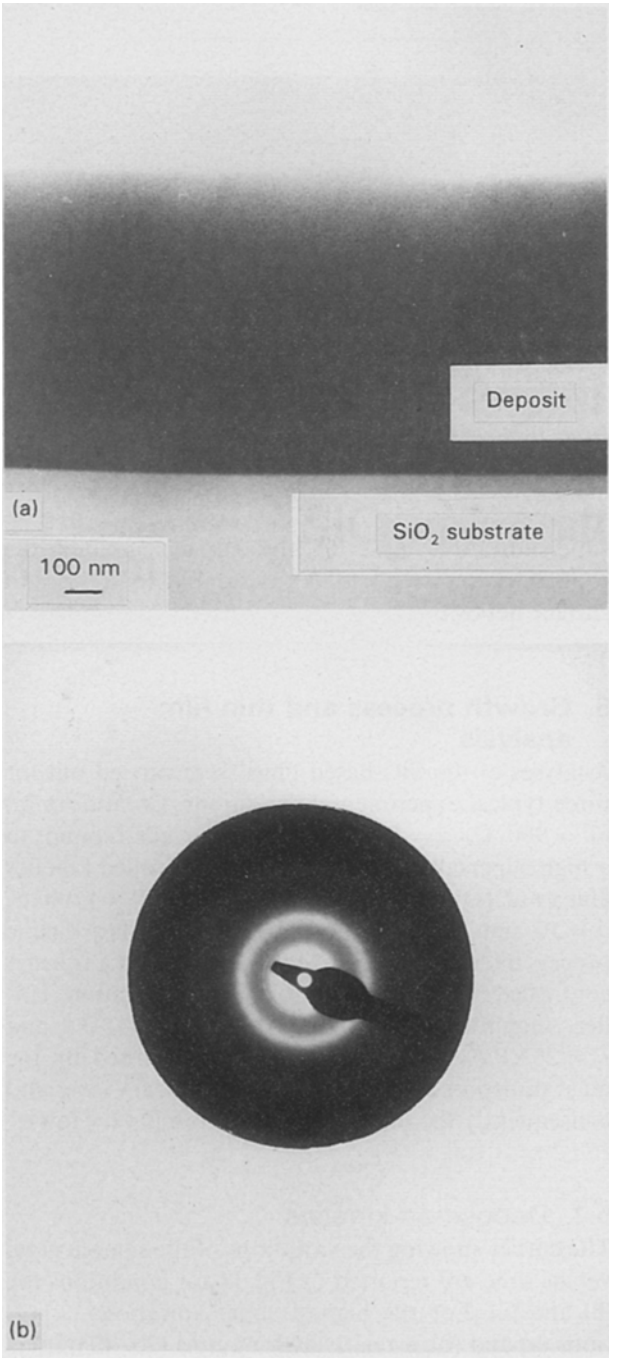

Figure 13 Bright-field image (a) and SAD pattern (b) of a SiC-based deposit on a SiO_2 substrate for $T = 900\,°C$, $\alpha = 3$ and $P = 3\,kPa$.

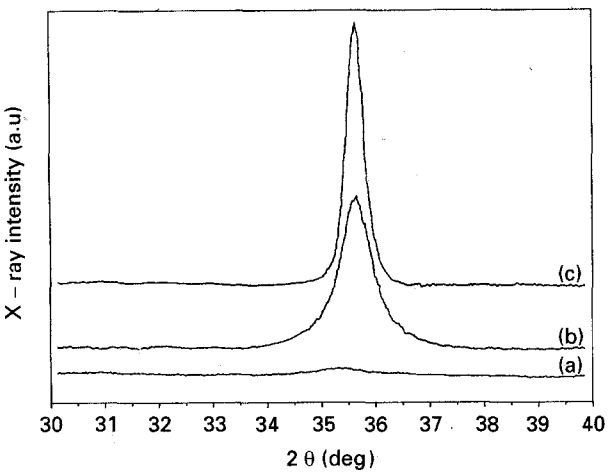

Figure 14 (1 1 1) X-Ray (CuK_α) diffraction peaks of SiC-based deposits obtained under various conditions: (a) $T = 900\,°C$, $\alpha = 3$, $P = 3$ kPa, (b) $T = 1100\,°C$, $\alpha = 10$, $P = 3$ kPa, (c) $T = 1100\,°C$, $\alpha = 3$, $P = 20$ kPa.

a marked surface roughness (Fig. 12c), a local analysis of the chemical composition is needed.

5.4. Chemical composition

Local EELS analyses were carried out as a function of d, the distance from the substrate/deposit interface. The relative concentrations of Si, C and O have been estimated through the quantitative exploitation of the corresponding core excitation signals, i.e. Si–L, C–K and O–K.

For the highest supersaturation (conditions (a)), Si and C are present in proportions above and below the values corresponding to stoichiometric SiC respectively (Fig. 17). This difference rises slowly but monotonously with d. At 1000 nm, silicon and carbon atomic concentrations are respectively 66 and 30%. In addition, a small quantity of oxygen is present in the deposit, which decreases with thickness to a few atomic percents.

For conditions (b) (Fig. 18), and for $d < 450$ nm (where nanocrystals are present), the situation is similar to the one of the highest supersaturation case near the silica substrate ($d < 100$ nm in Fig. 17). Beyond $d = 450$ nm, the silicon to carbon ratio moves towards the stoichiometric ratio when d increases and the oxygen content decreases to zero (at $d = 1000$ nm, 53 at% Si, 47 at% C).

From thermodynamic considerations, on the one hand, XRD and Raman spectroscopy microprobe experiments, on the other hand, carbon can be engaged only in silicon carbide and free silicon can be very often codeposited under conditions of relatively high supersaturation [15]. The same situation is observed in the two previous cases.

For a very low supersaturation, corresponding to conditions (c) (Fig. 16), columnar crystals are stoichiometric. The centre of the above described inclusions contains excess silicon. In the same way, the 30 nm thick nanocrystalline layer beside the substrate contains a slight excess of silicon.

5.5. Discussion

The SiC-based films deposited from a highly supersaturated gas phase (i.e. for conditions (a): $T = 900\,°C$, $\alpha = 3$ and $P = 3$ kPa) are found to be quasi-amorphous. They contain a silicon excess and a small amount of oxygen. The oxygen, probably due to a residual partial pressure in the reactor, can be easily incorporated between the numerous SiC-based nanocrystals. The important transient stage observed in the kinetic curve, can be compared to the profile of oxygen content within the film: the growth rate increases when the oxygen percentage decreases and both become constant after a deposition of about 750 nm in thickness. As will be discussed in a further paper, oxygen could act as inhibitor for the deposition of silicon carbide [27].

If the supersaturation is decreased (i.e. for conditions (b): $T = 1100\,°C$, $\alpha = 10$ and $P = 3$ kPa), the crystallization state is improved particularly in the upper layers of the film where the crystallites change from isotropic to columnar in connection with the content changes of Si, C and O discussed in Section 5.4.

Conditions (c) ($T = 1100\,°C$, $\alpha = 3$ and $P = 20$ kPa), for which the local supersaturation cannot be

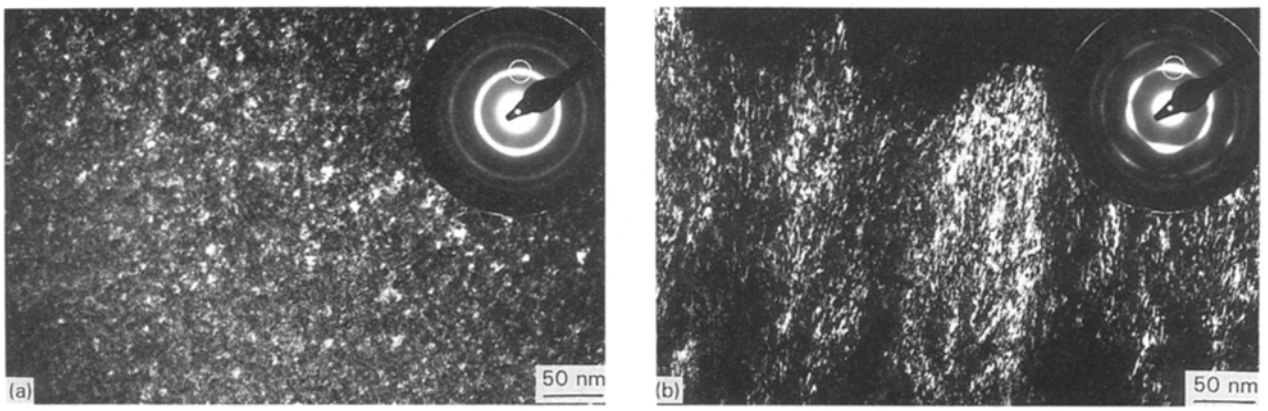

Figure 15 Dark-field images and SAD pattern inserts of a SiC-based deposit on a SiO_2 substrate for $T = 1100\,°C$, $\alpha = 10$ and $P = 3$ kPa, (a) near the substrate, (b) at 1 μm far from the substrate.

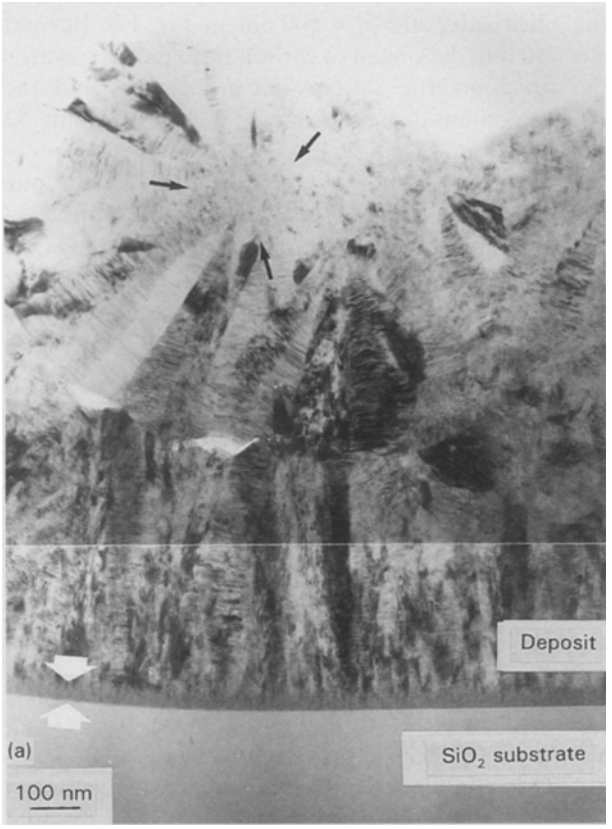

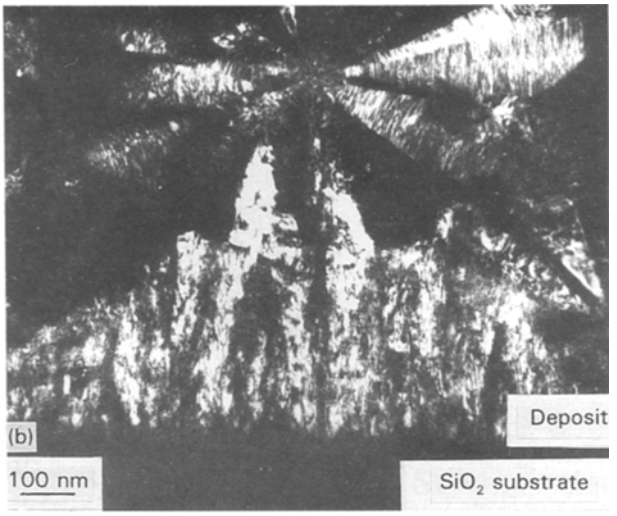

Figure 16 Bright-field (a) and dark-field (b) images of a SiC-based deposit on a SiO_2 substrate for $T = 1100\,°C$, $\alpha = 3$ and $P = 20\,kPa$. Black arrows show an inclusion containing silicon excess in its centre. White arrows show the thin nanocrystalline layer.

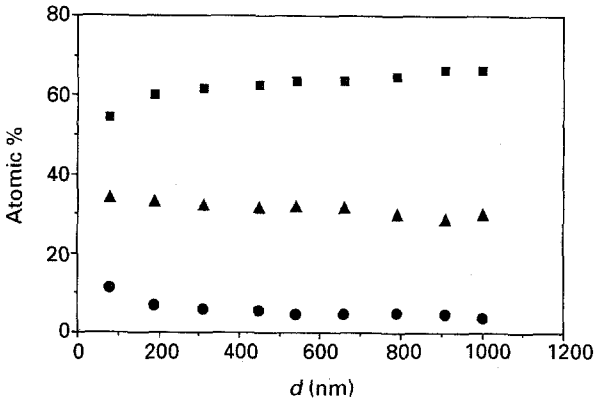

Figure 17 Variations of Si, C and O contents with the distance d measured between the analysed area and the substrate/deposit interface, in a SiC-based film obtained for $T = 900\,°C$, $\alpha = 3$, $P = 3\,kPa$. ■, Si; ▲, C; ●, O.

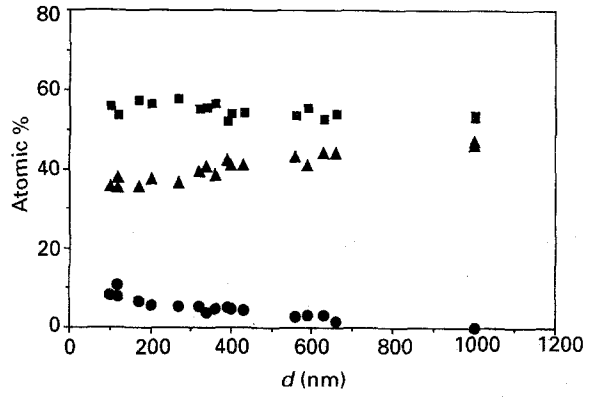

Figure 18 Variations of Si, C and O contents with the distance d measured between the analysed areas and the substrate/deposit interface, in a SiC-based film obtained for $T = 1100\,°C$, $\alpha = 10$, $P = 3\,kPa$. ■, Si, ▲, C; ●, O.

exactly calculated but is much lower than previously, result in drastically different deposition process and physico-chemcial characteristics of the film. First of all, the kinetics is totally controlled by the mass transport of reactive species through the boundary layer surrounding the substrate. The kinetic curve does not exhibit a transient stage and the film consists of stoichiometric silicon carbide except at the centre of the inclusions where free silicon is observed. The formation of these inclusions can be explained by assuming that silicon nuclei are homogeneously formed in the gas phase, owing to local large concentrations of silicon source species, such as $SiCl_2$. Some of these nuclei, which are stagnant in the boundary layer, act as small additional substrates for silicon carbide deposition. A radial growth of columnar SiC crystals occurs on these silicon cores. When the size of the resulting grains is high enough, some of them are evacuated down the reactor and the others are stuck on the sample surface, a feature which leads to the observed heterogeneity (Fig. 16). The growth discontinuity observed at the interface between the columnar layer on the substrate and the inclusions shows the independence of both growth processes. On the other hand, the radius of these inclusions is frequently found to be close to the thickness of the columnar sub-layer, which confirms that the homogeneous nucleation of silicon and the heterogeneous deposit of SiC on the substrate begin at the same time.

6. Conclusions

The present experimental investigation of the nucleation of growth and SiC-based ceramics from CH_3SiCl_3–H_2 precursor on SiO_2 substrate in conjunction with supersaturation assessments, permit us to suggest correlations between synthesis conditions and physico-chemical characteristics of the films

TABLE I Correlations between CVD conditions, kinetic regime, supersaturation, nucleation and physicochemical characteristics of SiC-based films; *overestimated value of the local supersaturation (see Section 3.1)

T (°C)	900	1100	1100
α	3	10	3
P (kPa)	3	3	20
Kinetic control	Surface reactions	Surface reactions + Mass transport	Mass transport
Local supersaturation	1.3×10^6		(9.6×10^4)*
$I(m^{-2}s^{-1})$	1.7×10^{13}		7×10^{10}
$N_s(m^{-2})$	1.5×10^{14}		6.5×10^{12}
Φ_s(nm)	40		200
Surface morphology	Smooth	Rough	Angular
Microstructure	Nanocrystalline and isotropic	Nanocrystalline and textured	Large columnar crystallites
Chemical composition	SiC + Si O:12–4 at%		SiC stoichiometric 0 at%

(Table I). On the one hand, for a kinetic process controlled by the surface reactions, i.e. mainly for low temperatures and low total pressures, the supersaturation of the gas phase close to the substrate is very high ($\gamma > 10^5$), which favours a rapid continuous nucleation. These conditions give rise to a nanocrystallized SiC material including some excess of silicon and a small amount of oxygen, the surface morphology of the film being rather smooth. On the other hand, for a kinetic process controlled by mass transport through a boundary layer (i.e. for relatively high temperatures and total pressures), the local supersaturation cannot be calculated without a good knowledge of the boundary layer, but can be assumed to be rather low, which favours a growth regime instead of a nucleation process. Under these conditions, columnar SiC crystals can grow with relatively large heterogeneities, owing to silicon homogeneous nucleation followed by SiC growth in the stagnant gaseous layer. A rather rough surface morphology results from this process.

These results show that the supersaturation of the gas phase and the type of kinetic process involved in the deposition of SiC-based ceramics are determining factors for the control of their morphology and microstructure.

Acknowledgements

The authors wish to thank Dr C. Bernard (LTPCM, Grenoble) for his contribution to the thermodynamic calculations, F. Loumagne (LCTS, Pessac) for her help in the kinetic experiments, R. Fourmeaux and P. Salles (CEMES, LOE, Toulouse) for their support in electron microscopy experiments. This work has been supported by Société Européenne de Propulsion and CNRS (via a grant given to D. Lespiaux).

References

1. T. HIRAI and M. SASAKI, in "Silicon Carbide Ceramics-1", edited by S. Somiya and Y. Inomata (Elsevier Science Publishers, London, New York, 1991) p. 77.
2. R. NASLAIN and F. LANGLAIS, in "Tailoring Multiphase and Composite Ceramics", edited by R. E. Tressler, G. L. Messing, G. G. Pantano and R. E. Newnham (Plenum Publishing Corporation, 1986) p. 145.
3. J. SCHLICHTING, *Powder Metall. Int.* **12** 3 (1980) 141 and **12** 4 (1980) 196.
4. W. F. KNIPPENBERG, *Philips Res. Repts.* **18** (1963) 161.
5. S. HOTOJIMA, H. YAGI and N. IWAMOSI, *J. Mater. Sci. Lett.* **5** (1986) 13.
6. J. BLOEM, *Acta Electronica* **21** 3 (1978) 201.
7. W. A. P. CLAASSEN and J. BLOEM, *J. Electrochem. Soc.* **127** (1980) 194.
8. *Idem, ibid.* **127** (1980) 1336.
9. *Idem, ibid.* **128** (1980) 1353.
10. J. BLOEM, *J. Crystal Growth* **50** (1980) 581.
11. F. HOTTIER and R. CADORET, *J. Crystal Growth* **52** (1981) 199.
12. J. CHIN, P. K. GANTZEL and R. G. HUDSON, *Thin Solid Films* **40** (1977) 57.
13. R. PAMPUCH and L. STOBIERSKI, *Ceramurgia Int.* **3** 2 (1977) 43.
14. F. SIBIEUDE and G. BENEZECH. *J. Mater. Sci.* **23** (1988) 1632.
15. R. CADORET, in "Current Topics in Materials Science", edited by E. Kaldis (North-Holland, Amsterdam, 1980) ch. 2.
16. C. PREBENDE, Thesis no. 347, University of Bordeaux (1989).
17. F. LOUMAGNE, F. LANGLAIS and R. NASLAIN, *J. le Physique IV*, 3/C3 (1993) 527.
18. F. LANGLAIS, F. HOTTIER and R. CADORET, *J. Crystal Growth* **56** (1982) 659.

19. F. LANGLAIS and C. PREBENDE, in Proceedings of Eleventh International Conference on CVD, Seattle, October 1990, edited by K. E. Spear and G. W. Cullen (The Electrochem, Society, Pennington, 1990) p. 686.
20. H. POPPA, *J. Appl. Phys.* **38** 10 (1967) 3883.
21. M. GISO and J. CHUN, *J. Vac. Sci. Technol. A* **6** 1 (1988) 5.
22. K. A. JACOBSON, *J. Electrochem. Soc.* **118** 6 (1971) 1001.
23. K. MINATO and K. FUKUDA, *J. Mater. Sci.* **23** (1988) 699.
24. P. TSUI and K. E. SPEAR, *Mat. Sci. Res.* **17** (1984) 37.
25. S. PROUHET, F. LANGLAIS, A. GUETTE, R. NASLAIN and J. REY, *Eur. J. Solid State Inorg. Chem.* **30** (1993) 953.
26. VON M. HORSTMANN and G. MEYER, *Acta Cryst.* **15** (1962) 271.
27. D. LESPIAUX, F. LANGLAIS, R. NASLAIN, S. SCHAMM and J. SEVELY, *J. Europ. Ceram. Soc.* (in press).

Received 12 October 1993
and accepted 11 August 1994